

IDENTIFICATION OF DEFECTS IN SILICON BY EPR AND ENDOR
- THE VACANCY IN SILICON -

C.A.J. Ammerlaan, M. Sprenger and E.G. Sieverts

*Natuurkundig Laboratorium der Universiteit van Amsterdam, Valckenierstraat 65,
1018 XE Amsterdam, The Netherlands*

In this paper, the identification and characterization of point defects in silicon by means of electron paramagnetic resonance and electron-nuclear double resonance is discussed. The vacancy in silicon is taken as the example to illustrate the elucidation of the atomic and electronic structure from the data obtained by magnetic resonance.

1. Introduction

1.1. Introduction to the vacancy in silicon

When creating a vacancy, an empty atom site in a crystal, the bonds between the atom which is removed and its former nearest-neighbour atoms are disrupted. In a covalent crystal, such as silicon, two electrons occupy the bonding orbital between any two neighbouring atoms, with their spins paired-off. Around a vacant site in the diamond structure, in which silicon crystallizes, the four nearest-neighbour atoms are left with unpaired electrons in dangling bonds. These sp^3 -hybridized orbitals point towards the vacancy centre. To reduce the energy of the defect, the overlap between the dangling bonds will be optimized by relaxation of atom positions. Allowance is thereby made for the energy in the backbonds of the neighbour atoms and further bonds in the vicinity. In the process of bond reconstruction the atoms around the vacancy will distort from the

geometrical crystal positions for silicon, in a way which may lower the symmetry of the defect. With the new bonds, energy levels in the bandgap of the semiconductor silicon are associated. The occupation of these bonds, and hence the charge state of the vacancy, will depend on the position of the Fermi level with respect to the defect levels.

Figure 1 summarizes the atomic and electronic characterization of the lattice vacancy. In the doubly positively charged state of the vacancy, the undistorted cubic symmetry of the silicon crystal is retained, with point-group symmetry $\bar{4}3m$ for the defect site. In a simple model, the defect molecule consisting of the four dangling bonds associated with the silicon nearest neighbours around the vacant site is considered [1,2]. The sp^3 -hybridized orbitals centered on these neighbours are labelled a, b, c and d. The four basis functions in $\bar{4}3m$ symmetry, constructed as linear combination of these atomic orbitals, LCAO, transform as an a_1 -singlet or as a t_2 -triplet. For V^{++} , with two electrons in the defect molecule, the lowest two spin-orbitals, of the totally-symmetric orbitally a_1 -type, are occupied. A breathing mode distortion, which does not affect the symmetry, will occur. By adding one electron, in going from V^{++} to V^+ , the t_2 -level becomes singly occupied. The Jahn-Teller theorem states that the partially occupied orbitally-degenerate level is unstable. A spontaneous distortion, resulting in lowering of the electronic energy, is to be expected. In the case of the vacancy, a tetragonal distortion to point-group symmetry $\bar{4}2m$, as indicated in figure 1 for V^+ , will occur. The distortion lifts the three-fold degeneracy of the t_2 -level. The third vacancy electron of V^+ will be accommo-

Charge state	Point-group	Levels and occupation	Symmetry-type	LCAO of a, b, c and d	Model
v^-	$2m$		b_2	$b-c$	
			b_1	$a-d$	
			a_1''	$(a+d)-\lambda(b+c)$	
			a_1'	$\lambda(a+d)+(b+c)$	
v^0	$\bar{4}2m$		e	$a-b+c-d$ $a+b-c-d$	
			b_2	$a-b-c+d$	
			a_1	$a+b+c+d$	
v^+	$\bar{4}2m$		e	$a-b+c-d$ $a+b-c-d$	
			b_2	$a-b-c+d$	
			a_1	$a+b+c+d$	
v^{++}	$\bar{4}3m$		t_2	$a-b-c+d$ $a-b+c-d$ $a+b-c-d$	
			a_1	$a+b+c+d$	

Figure 1. Electronic structure of the vacancy in silicon, in various charge states and corresponding distortions, with LCAO's from the nearest neighbours a, b, c and d.

dated in the b_2 -type level, with orbital a-b-c+d in the nearest-neighbour LCAO model. The distribution of unpaired spin, equally over the four neighbours, is indicated by the shading in figure 1. For the neutral vacancy, the four electrons in the defect molecule occupy the lowest levels a_1 and b_2 in pairs, with spin-up and spin-down compensated. The Jahn-Teller distortion, as experienced for V^+ , will be amplified because two electrons now occupy the b_2 -level, which lowers its energy upon distortion. The symmetry will remain the tetragonal $\bar{4}2m$. Actually, the charge state V^+ is unstable, as the transfer of one electron between two positive vacancies in the reaction $2V^+ \rightarrow V^{++} + V^0$ yields an energetically more favourable situation. The lowering of energy associated with distortion outweighs the Coulomb repulsion between electrons, resulting in so-called negative U [3,4]. In spite of its instability, the positive vacancy can exist under non-equilibrium conditions, e.g. after creating this charge state by illumination. Its lifetime can be long enough for study of its properties. For the negative vacancy, the fifth electron in the defect molecule has to be put in the next available level, which is the e-level. The partial occupation of an orbitally degenerate level again induces a Jahn-Teller instability, with further distortion and lifting of the electronic degeneracy. For V^- this results in rhombic symmetry, point-group $2mm$. The LCAO basis-functions constructed from the nearest-neighbour orbitals are indicated in figure 1. The wavefunctions are given in non-normalized form. Parameter λ , which measures the mixing between the two a_1 -type levels depends on the rhombic distortion. The spin density, indicated by shading the orbital, is mainly

concentrated on two of the neighbour atoms, forming the orbital of irreducible representation b_1 .

In the model considered, a defect molecule with covalent bonding, the charge states of the vacancy with an odd number of electrons are predicted to be paramagnetic, with $S=1/2$. For V^+ , with three electrons, and V^- , with five electrons, electron paramagnetic resonance has indeed been observed [5]. The spectra are designated Si-G1 and Si-G2, respectively [6].

1.2. Introduction to magnetic resonance

Magnetic resonance is the resonant absorption and emission of power from electro-magnetic radiation when transitions are induced between the energy levels of a magnetic system. In solids, the main contribution to the magnetism arises from the unpaired spins and orbital moments of electrons. In this case, the magnetic moments are of order of magnitude of the Bohr magneton $\mu_B = 9.27 \times 10^{-24}$ J/T. The magnetic levels can be separated in energy through the Zeeman effect, by applying an external magnetic field. Transitions between these levels give the electron paramagnetic resonance, EPR, spectrum. Nuclear magnetic moments, from nuclei with $I \neq 0$, may be present in addition. Their contribution to the magnetization, of order of the nuclear magneton $\mu_N = 5.05 \times 10^{-27}$ J/T, is much smaller than the electronic part in a paramagnetic centre. The nuclei, with their magnetic moments $\vec{\mu}_n = g_n \mu_N \vec{I}$, will interact with the electronic moments $\vec{\mu}_e = -g_e \mu_B \vec{S}$, when sufficiently close. This will cause the hyperfine structure in the resonance spectrum.

The relevant energies for the magnetic system with one electronic and one nuclear spin are then given by the spin-

Hamiltonian

$$H = g_e \mu_B \vec{B} \cdot \vec{S} - g_n \mu_N \vec{B} \cdot \vec{I} + a \vec{S} \cdot \vec{I}. \quad (1)$$

For simplicity all interactions have been assumed to be isotropic. For lowest values of the spins, $S=1/2$ and $I=1/2$, the four basis states are $|m_S, m_I\rangle = |\pm 1/2, \pm 1/2\rangle$. Energy eigenvalues are found by diagonalizing the 4×4 matrix of H in these basis states. For conditions of strong magnetic field, both spins are quantized along the magnetic field direction and the energy solutions are given, to first order by

$$E = g_e \mu_B B m_S - g_n \mu_N B m_I + a m_S m_I. \quad (2)$$

The corresponding energy level diagram is shown in figure 2.

In electron paramagnetic resonance a spin flip is induced between states with $m_S = +1/2$ and $m_S = -1/2$, while keeping the nuclear magnetic quantum number m_I unchanged. The condition for resonance is derived by equating the quantum of energy involved

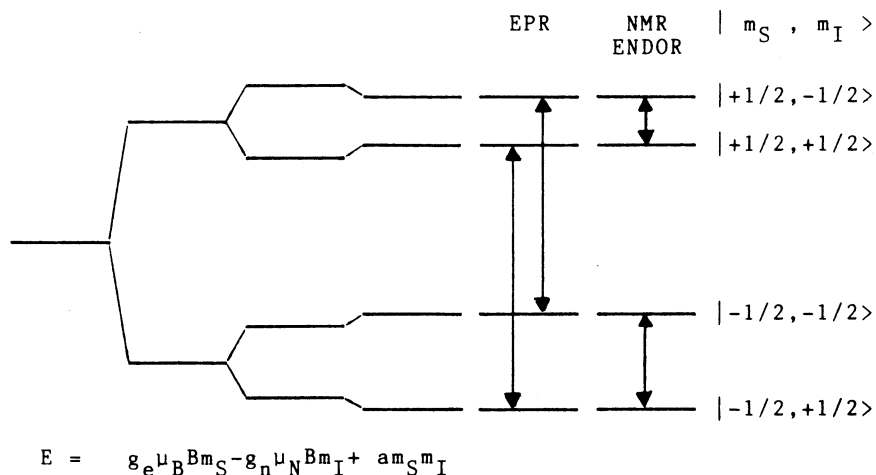


Figure 2. Level scheme with electronic magnetic energies applicable to Si:V^+ and Si:V^- with $S=1/2$, and with nuclear magnetic energies for one ^{29}Si -nucleus with $I=1/2$. The EPR, NMR and ENDOR transitions are indicated by the double-sided arrows.

in inducing the transition to the change of energy in the magnetic system. This gives

$$h\nu = g_e \mu_B B + a m_I. \quad (3)$$

Observation of the resonance allows the g-factor g_e , which serves as a unique spectroscopic characterization of the spectrum, to be determined. The hyperfine structure of the spectrum consists of $2I+1$ lines, corresponding to all possible values of m_I . When resolved, a simple count of the number of hyperfine components suffices to determine the nuclear spin I . The illustration in figure 3 gives the EPR spectrum of the negative vacancy in silicon. The EPR lines are accompanied by satellites, split off symmetrically, due to the interaction with ^{29}Si nuclei, which have $I=1/2$. The relative intensities of the main line and the satellites reflect the abundancies of the isotopes ($^{28}\text{Si}, I=0, 92.2\%$; $^{29}\text{Si}, I=1/2, 4.7\%$; $^{30}\text{Si}, I=0, 3.1\%$).

The corresponding case of nuclear magnetic resonance, NMR, is treated on an equal basis. From the selection rule $\Delta m_S=0$, $\Delta m_I=\pm 1$, the resonance condition follows:

$$h\nu = |g_n \mu_N B - a m_S|. \quad (4)$$

In general, the relative magnitude of the nuclear Zeeman effect $g_n \mu_N B$ and the hyperfine coupling $a m_S$ can differ and, therefore, the absolute bars have been used. To be specific for studies of centres in silicon, the important example of hyperfine interaction with ligand ^{29}Si nuclei, $I=1/2$, is now considered in some detail. For the conditions of measurement as in the example of figure 3, the EPR of the negative vacancy, with g-values close to 2, is found near $B=0.8$ T. The nuclear Zeeman frequency $g_n \mu_N B/h$ then is near 7 MHz. Only the strong hyperfine interactions with ^{29}Si nucleus on the nearest neighbour sites, a and

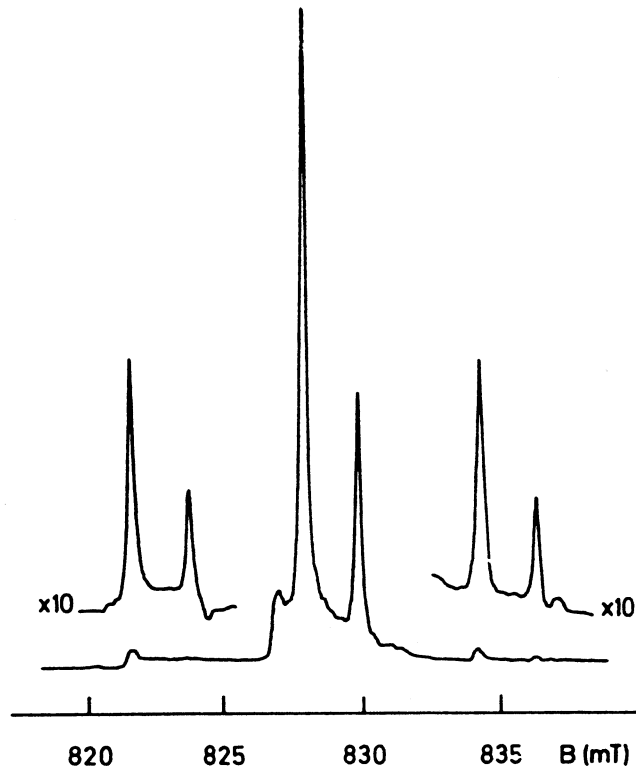


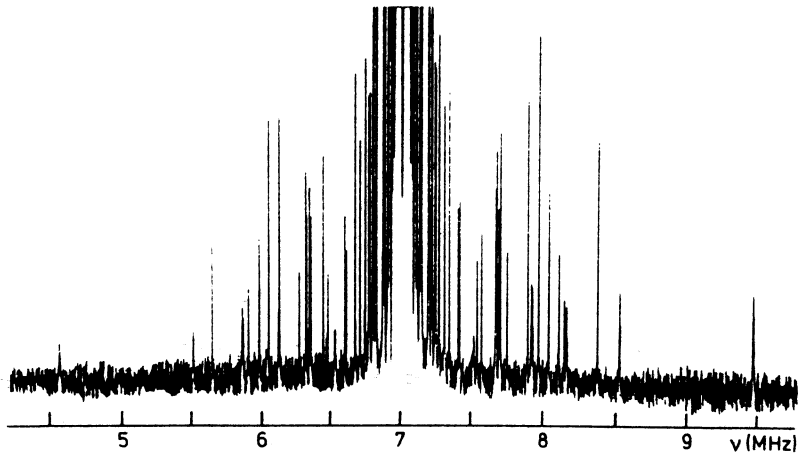
Figure 3. EPR spectrum of the negative vacancy in silicon, measured at temperature $T \approx 18\text{K}$, microwave frequency $\nu = 23.218\text{ GHz}$ and magnetic field \vec{B} parallel to crystal direction $\langle 100 \rangle$. The strongest hyperfine interactions with ^{29}Si -nuclei on sites a and d are resolved and also shown with gain 10x increased.

d in figure 1, are completely resolved in the EPR spectrum. The corresponding values of $a m_S/h$ are $\approx 180\text{ MHz}$, much larger therefore, than 7 MHz . For all other atom sites the hyperfine constant a is much smaller; actually, for most $a m_S/h < 7\text{ MHz}$, as the contact of the defect electron with the farther-away nuclei is less probable. For these interactions the NMR spectrum is symmetric around $\nu_Z = g_n \mu_N B/h$, with the higher and lower frequencies corresponding to $m_S = \pm 1/2$ in equation 4. A spectrum showing

this feature, actually taken from ENDOR on the negative vacancy, is given as figure 4(a) [7]. Obviously, from the nuclear Zeeman frequency ν_Z and the magnetic field B , which both can be measured with great precision, the nuclear g -factor g_n can be calculated. For the spectrum in figure 4(a) it follows from $\nu_Z = 7.0027$ MHz and $B = 0.82782$ T: $|g_n| = 1.1097$. This serves as an unambiguous identification of the nucleus involved in the resonance experiment. Of course, in the present example this merely confirms the known fact that one is dealing with the ^{29}Si isotope. In other cases, the chemical impurity forming a constituent of a paramagnetic centre may be unknown. Then, the determination of g_n by NMR (ENDOR) provides the identification. A recent example is the demonstration that boron is part of the centre from which the Si-G10 EPR spectrum arises [8,9].

In electron-nuclear double resonance, ENDOR, the two basic resonance phenomena, EPR and NMR, are performed simultaneously. The conditions have to be chosen so that the two resonances are interdependent, e.g. by spin-spin relaxation or by saturation of the population of levels. Technically, in ENDOR the effect of inducing an NMR transition is observed by a consequent change in the intensity of the EPR signal. Spectroscopically, ENDOR is identical to NMR and the resonance condition of equation 4 therefore applies. The superior energy resolution of NMR compared to EPR also positively features ENDOR. A linewidth of <1.5 kHz, shown in figure 4(b) for ENDOR, would correspond to a linewidth of <0.05 μT in EPR, as compared to an actual linewidth of typically 100 μT . The ENDOR sensitivity can approach that of EPR and, therefore ENDOR can be observed when NMR signals are far below the detection limits. This, however, de-

(a)



(b)

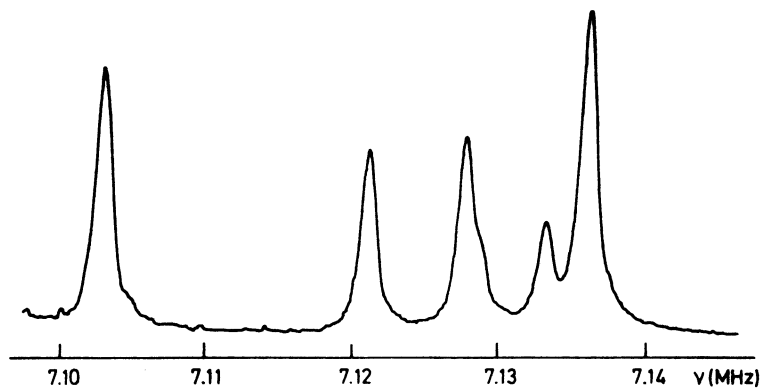


Figure 4. (a) A low-resolution ENDOR spectrum for the negative vacancy in silicon showing the symmetry around the nuclear Zeeman frequency, (b) Part of the same spectrum recorded under conditions of best resolution with linewidths less than 1.5 kHz.

depends crucially on whether suitable conditions for simultaneous electronic and nuclear resonances do exist. A thorough search for ENDOR of the positive vacancy in silicon recently remained unsuccessful. An obvious other prerequisite for ENDOR is the presence of a nuclear magnetic moment in the paramagnetic centre, i.e. both S and I have to be non-zero.

2. Characterization of the vacancy in silicon by EPR and ENDOR

2.1. Point-group symmetry

As discussed in 1.1 the point-group symmetry of the positive vacancy is $\bar{4}2m$, whereas for the negative vacancy it is $2mm$. Since these are subgroups of the crystallographic symmetry $\bar{4}3m$ of silicon, the vacancy can be accommodated in the host crystal in several orientations. This orientational degeneracy is 3 for the positive vacancy; it is 6 for the negative vacancy. When measuring the angular variation of the resonance fields typical patterns are observed which reflect the symmetry classification. In Table I these symmetry properties are summarized. The angular dependences of the effective g-values for the vacancy as shown in figure 5 agree with the defect symme-

Table I. Symmetry classification of centres in silicon.

System	Point-group(s)	Resonances in direction		
		$\langle 100 \rangle$	$\langle 111 \rangle$	$\langle 011 \rangle$
Cubic	$\bar{4}3m, 23$	1	1	1
Tetragonal	$\bar{4}2m, \bar{4}$	2	1	2
Rhombic I	$2mm$	2	2	3
Rhombic II	222	3	1	3
Trigonal	$3m, 3, \bar{3}m, \bar{3}$	1	2	2
Monoclinic I	$2/m, m$	2	3	4
Monoclinic II	2	3	2	4
Triclinic	$1, \bar{1}$	3	4	6

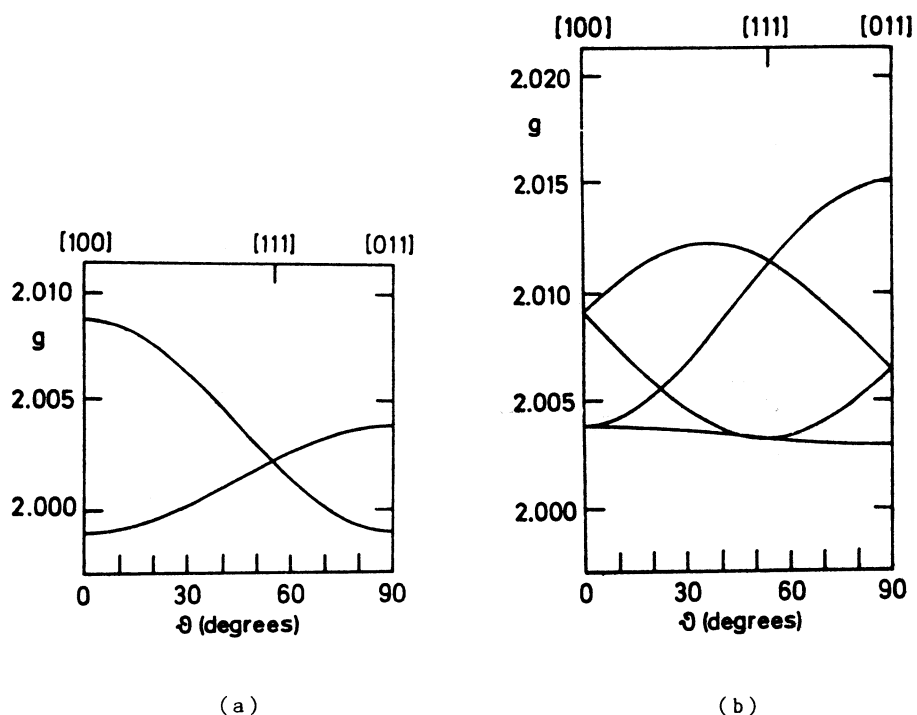


Figure 5. Angular variation for \vec{B} in the (011)-plane of the effective g-values of (a) the EPR-spectrum Si-G1 associated with Si:V⁺, and (b) the EPR-spectrum Si-G2 of Si:V⁻.

try. Actually, it is this experimental information from magnetic resonance from which the established defect symmetry was really derived.

In ligand ENDOR, the hyperfine interaction with a ^{29}Si nucleus is measured. In that case, the ^{29}Si nucleus is an integral part of the magnetic system. Depending on its position with respect to the vacancy, all symmetry transformations of $\bar{4}2m$ for V⁺ or $2mm$ for V⁻ may be retained, or some, or all, may be destroyed. For instance, for Si:V⁻ with the rhombic $2mm$ symmetry, the four distinct types of nuclear site are: on none of the two mirrorplanes, on one of each of the two non-equiva-

lent mirrorplanes, or on both mirrorplanes. The resulting combined symmetry for (vacancy+ ^{29}Si -nucleus) will be triclinic, monoclinic I, monoclinic I, or rhombic I, respectively. The angular patterns of the hyperfine interaction with the ^{29}Si -nuclei in shells of symmetry-related sites will reveal these symmetries. For $\text{Si}:\text{V}^-$, the hyperfine interactions were measured by ENDOR for 51 shells of atom sites around the defect [7,10]. Of these, 26 belong to the G-class of triclinic symmetry, 18 to the M_{ad} -class, 5 to the M_{bc} -class, both of monoclinic I symmetry, and 2 to the T-class with rhombic I symmetry. For the largest interaction in each class the results are shown in figure 6. In this way, ENDOR confirms convincingly the symmetry classification, already known from EPR. Because of the excellent resolution of ENDOR and the availability of many shells of hyperfine atoms, misinterpretation due to accidental degeneracies or lack of resolution is avoided.

2.2. Extension of the wavefunction

In the electronic model of the vacancy, as discussed in 1.1, the defect molecule including dangling bonds on only the four nearest neighbours of the vacancy was introduced. In figure 1, LCAO wavefunctions constructed correspondingly were given. From the ENDOR observations on 51 shells, containing 152 atoms around the negative vacancy, it is, however obvious that the defect electron penetrates measurably much deeper into the crystal. A more appropriate wavefunction will, therefore include orbitals on these sites and is written as

$$\psi = \sum_i \eta_i (\alpha_i \chi_{3s} + \beta_i \chi_{3p}). \quad (5)$$

The summation by i runs over atom sites around the vacancy, on

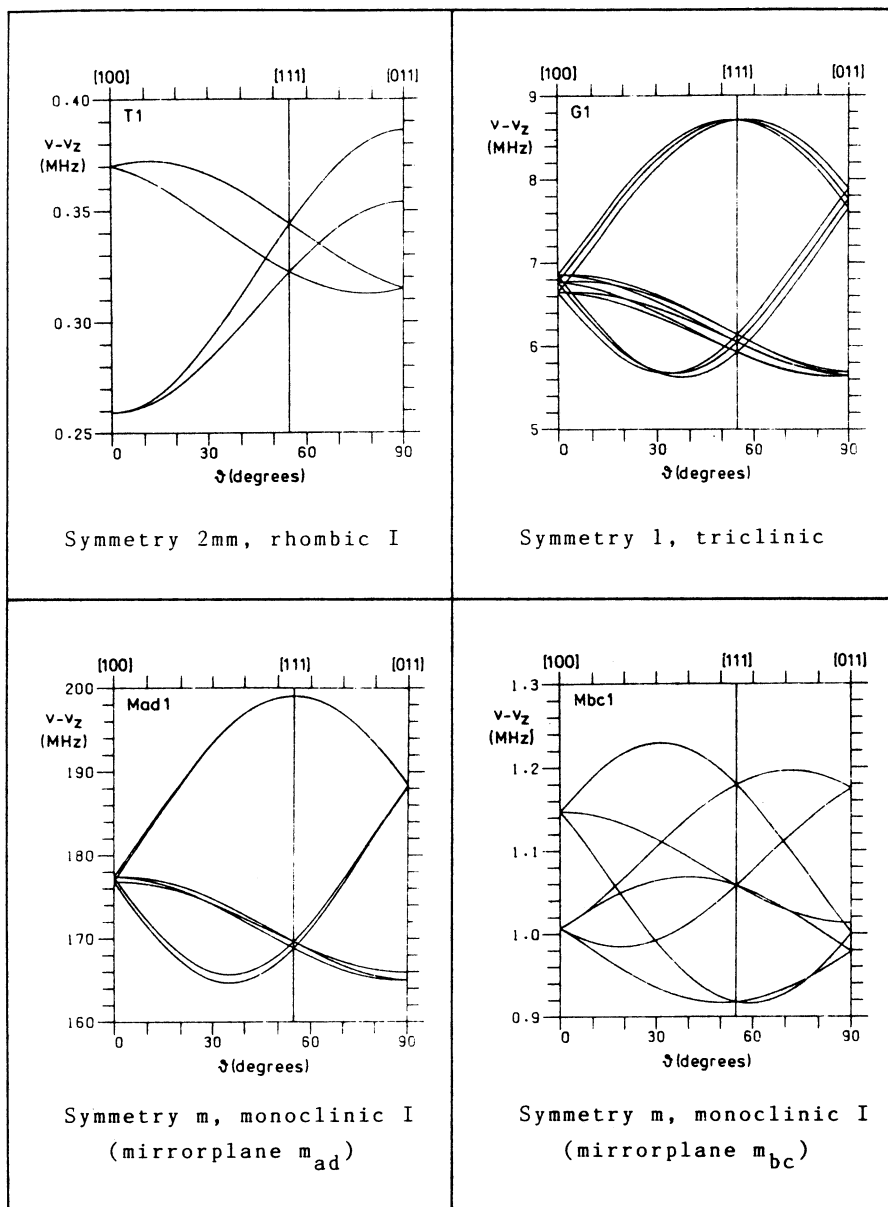


Figure 6. Angular dependence, for \vec{B} in the $(0\bar{1}1)$ -plane, of the hyperfine interaction frequencies $\nu - \nu_z$ for the triclinic, monoclinic I and rhombic I class shells for the negative vacancy in silicon. The largest tensor in each class is shown.

which 3s and 3p wavefunctions for silicon are included in the expansion. With the normalization $\alpha_i^2 + \beta_i^2 = 1$ the localization of the defect electron on site i is given by η_i^2 . In terms of the wavefunction ψ the hyperfine interaction can be calculated, establishing relations between the coefficients $\eta_i \alpha_i$ and $\eta_i \beta_i$ in the expansion and the constants in the measured hyperfine tensors. On the basis of a wavefunction given in equation 5, axial forms of the tensors are expected. The isotropic parts $a_i = (1/3) \text{Tr}(\hat{A}_i)$ of these tensors are interpreted as resulting from contact interaction. Dipole-dipole interaction between the electronic and nuclear moments results in traceless axial tensors. The main contribution arises from the orbitals centered on the site of the ^{29}Si -nucleus. In this approximation the isotropic parts a_i are then related to the s-functions by

$$a_i = (2/3) \mu_o g_e \mu_B g_n \mu_N \alpha_i^2 \eta_i^2 |\chi_{3s}(0)|^2. \quad (6)$$

From the p-functions axial tensors \hat{B} , with principal values $(b_i, b_i, -2b_i)$ originate with

$$b_i = (2/5) (\mu_o / 4\pi) g_e \mu_B g_n \mu_N \beta_i^2 \eta_i^2 \langle 1/r^3 \rangle_{3p}. \quad (7)$$

Using as estimates for the atomic parameters $|\psi_{3s}(0)|^2 = 34.52 \times 10^{30} \text{ m}^{-3}$, $\langle 1/r^3 \rangle_{3p} = 18.16 \times 10^{30} \text{ m}^{-3}$ [11], the wavefunction coefficients η_i , α_i and β_i can be calculated.

Having obtained this information on the distribution of the defect electron over atomic sites around the vacancy, still the assignment of hyperfine tensors \hat{A} or coefficients η_i , α_i and β_i to specific shells, or atom sites, is not known. Apart from the classification into general sites, mirrorplane sites and sites on the twofold axis such an assignment does not follow from the ENDOR information. A general theory for defect states providing the lacking information also does not exist.

In order to proceed with the interpretation to obtain a rough mapping of the defect electron, an ad hoc assumption has to be made. A reasonable one is to assume monotonic decrease of the wavefunction ψ with distance $|\vec{r}|$ to the vacancy within the symmetry classes, although violations of this rule will certainly occur. Nevertheless adopting this view, data for the negative vacancy in silicon, η_1^2 versus r_1 , are presented in figure 7. Fits with exponential functions

$$\eta^2 = \eta_0^2 \exp(-2r/r_0) \quad (8)$$

are included in the figure. The pre-exponential density parameter η_0^2 and the characteristic decay length r_0 for best match are given in table II. One finds $r_0 \approx 3 \times 10^{-10}$ m, much smaller than the 15×10^{-10} m which the effective mass theory predicts for shallow donors and acceptors. This result confirms that defects with deep electronic levels, such as the vacancy, have much more localized bound electrons than shallow states.

Table II. Parameters for the wavefunction of the negative vacancy in silicon. See text for assignment of tensors to shells.

Class	η_0^2	r_0 (10^{-10} m)	Model
M_{ad}	0.72	2.9	Ordering with- in classes
G	0.23	2.7	
M_{bc}	0.029	3.1	
M_{ad}	0.39	5.1	[011] chain

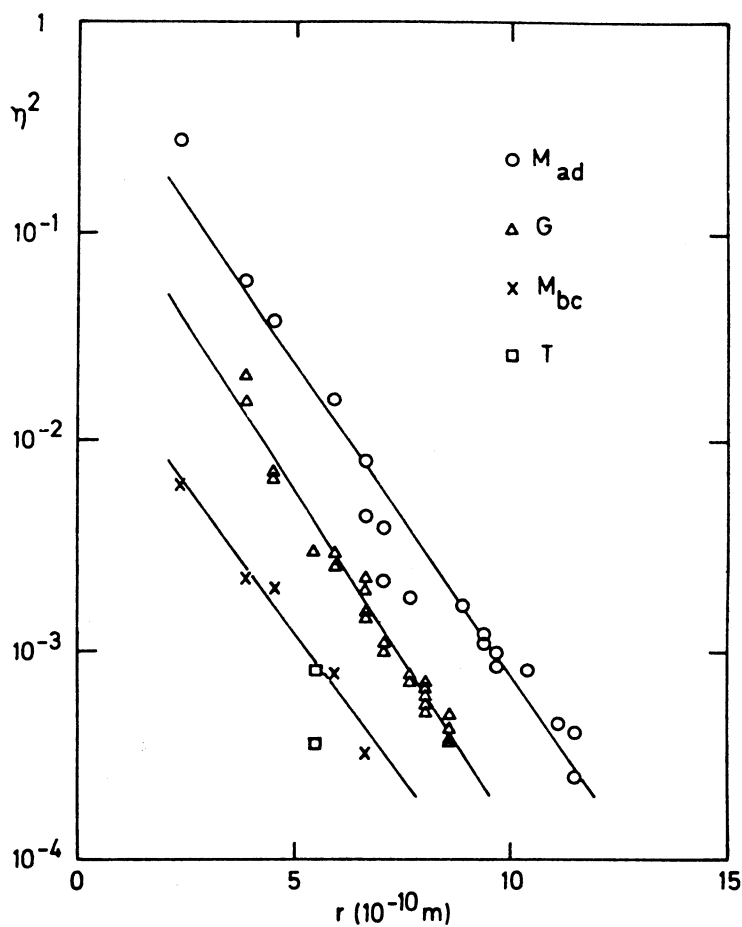


Figure 7. The localization η_i^2 of the wavefunction of the negative vacancy in silicon as a function of the distance r_i to the vacancy site, with ordering of sites in symmetry classes.

2.3. Shape of the wavefunction

Inspection of figure 7 clearly shows the inequivalence of the two mirrorplanes m_{ad} and m_{bc} . Whereas for m_{ad} the density parameter $\eta_0^2 \approx 0.72$, for m_{bc} it is only 0.029 (table II). Therefore the ENDOR data inevitably show a strong localization of the wavefunction on one plane. Rather than being spherically

distributed around the point defect, as sketched in figure 11(a), the charge and spin of the defect electron is quite flat, as in figure 11(b).

This interpretation on an empirical basis may be carried one step further. Careful inspection of the hyperfine tensors in the M_{ad} class reveals striking similarities between several of them. It appears that the tensors $M_{ad}1, 2, 3, 4, 5, 6, 8, 12, 14,$ and 17 have their principal axes all very nearly parallel and, moreover, have nearly equal a_i/b_i -ratio. This suggests a relation between these tensors and associated lattice sites, as could result from transferred spin density along an atom chain. Chains which zig-zag along $\langle 011 \rangle$ directions are prominent in the covalent silicon lattice. A plot of η_1^2 for these tensors as function of distance r_i , with atom sites taken along the $[011]$ chain in the m_{ad} -plane, as given in figure 8, results in a rather perfect exponential decay. The characteristic decay length $r_0 = 5.1 \times 10^{-10}$ m (table II), following from the straight line fit is appreciably larger than the average "isotropic" decay length. The observed exponential decrease for a wavefunction outside the potential well is in agreement with the general theoretical notions. The enhanced linear extension is also supported by a recently developed very specific model [12]. Here the picture emerges of spin density not just localized in one plane, as in figure 11(b), but rather stretched along one chain, as drawn in figure 11(c).

2.4. Symmetry type of the wavefunction

A striking aspect of the ENDOR results is the marked inequivalence of the two mirrorplanes in the $2mm$ point-group. A

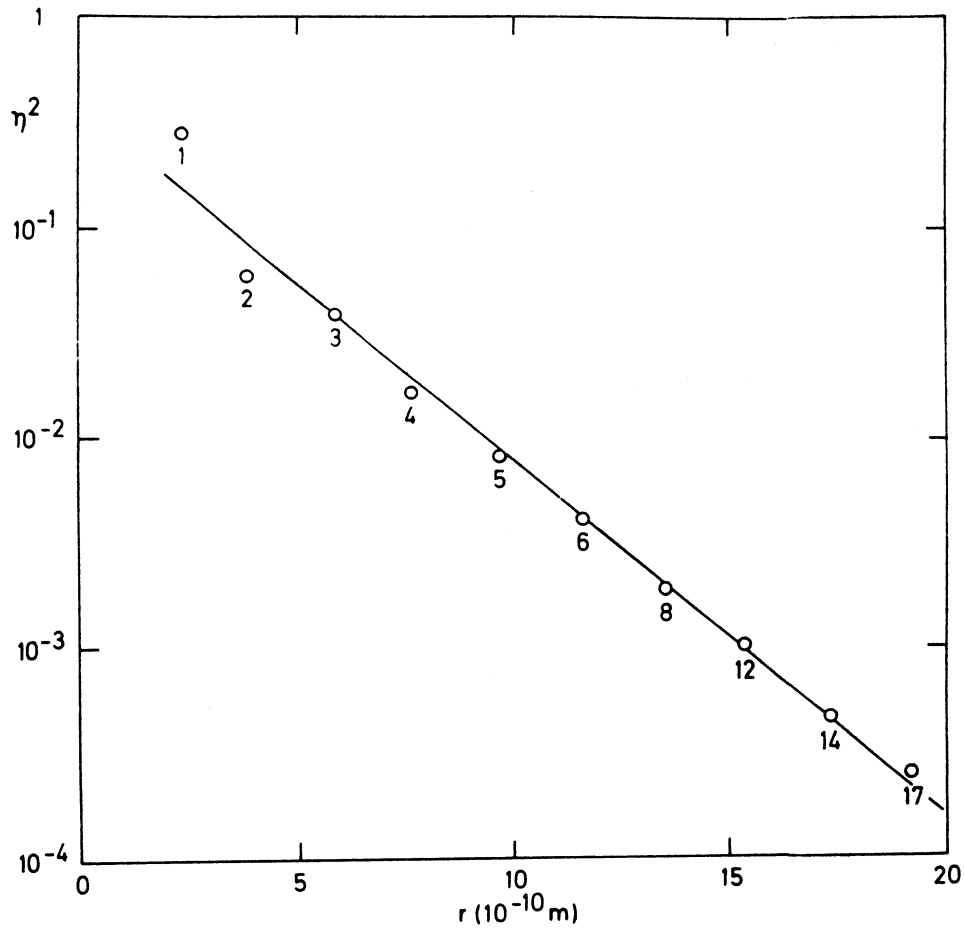


Figure 8. The localization η_i^2 of the wavefunction of the negative vacancy in silicon as a function of the distance r_i to the vacancy site, for ordering along the [011] chain.

strong contact interaction, i.e. large values for $\eta_i^2 \alpha_i^2$, is observed for sites in the m_{ad} -plane, implying even symmetry, or s-character, for reflection in this plane. Contrary to this, for the m_{bc} -plane, the values $\eta_i^2 \alpha_i^2$ are very small. For an interpretation they are therefore considered to be essentially zero. A vanishing density in the bc-plane, i.e. a node of the wave-

function in the bc-plane, implies odd symmetry, or p-character, with respect to this plane. Figure 9 illustrates the reflection characters of the 4 symmetry-types of point-group $2mm$ pictorially. Only symmetry-type b_1 is compatible with the ENDOR results for Si:V^- . Thus, the detailed and accurate results of ENDOR allow the symmetry-type of the wavefunction to be determined. The ensuing b_1 -type for the negative vacancy in silicon supports the theoretical electronic nearest-neighbour LCAO

Symmetry-type	Characters				Diagram
	E	m_{ad}	m_{bc}	2	
a_1	1	1	1	1	
a_2	1	-1	-1	1	
b_1	1	1	-1	-1	
b_2	1	-1	1	-1	

Figure 9. Characters of the various symmetry-types in point-group $2mm$ for reflection in the mirrorplanes m_{ad} and m_{bc} .

model as presented in paragraph 1.1 and figure 1. A corresponding distribution of the charge density is given in figure 11(d).

2.5. Many-electron wavefunction

Although, as discussed in the previous paragraph, the contact hyperfine interactions with nuclei in the bc-plane are very small, they are not exactly zero. This violation of the symmetry requirements for a b_1 -type wavefunction can be understood in a many-electron description. So far, the ground-state of the 5 electrons in the defect molecule for $\text{Si}:\text{V}^-$ has been considered, represented by the wavefunction $\psi_0 = |a_1' \bar{a}_1' a_1'' \bar{a}_1'' b_1\rangle$ and illustrated in figure 1. Through the polarizing effect of the unpaired electron in the b_1 -orbital, excited states with the same 2B_1 symmetry will be admixed into the groundstate ψ_0 . Such excited states, within the nearest-neighbour LCAO model, are $\psi_1 = |a_1' \bar{a}_1' b_1 b_2 \bar{b}_2\rangle$, $\psi_2 = |a_1'' \bar{a}_1'' b_1 b_2 \bar{b}_2\rangle$, $\psi_3 = |a_1' \bar{a}_1'' b_1 b_2 \bar{b}_2\rangle$ and

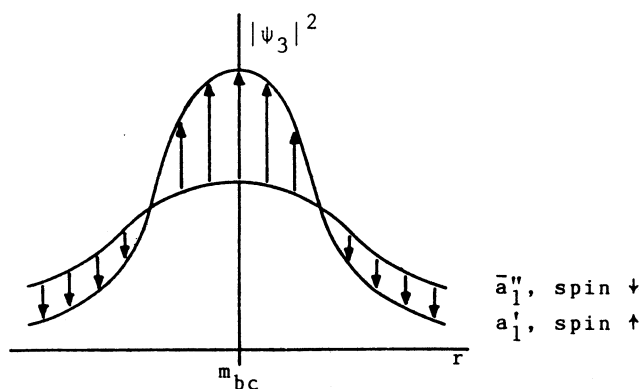


Figure 10. Spatial distribution of spin-density around the bc-plane with opposite spin in the a_1' and a_1'' orbitals.

$\psi_4 = |\bar{a}_1' a_1'' b_1 \bar{b}_2\rangle$. Both the configurations ψ_3 and ψ_4 have non-zero spin density on the bc-plane as the spin in the a' -orbital will not be cancelled by the opposite spin in the a'' -orbital, as figure 10 illustrates. An unequal admixture of the states ψ_3 and ψ_4 into the groundstate, which requires $\lambda \neq 1$, will result in

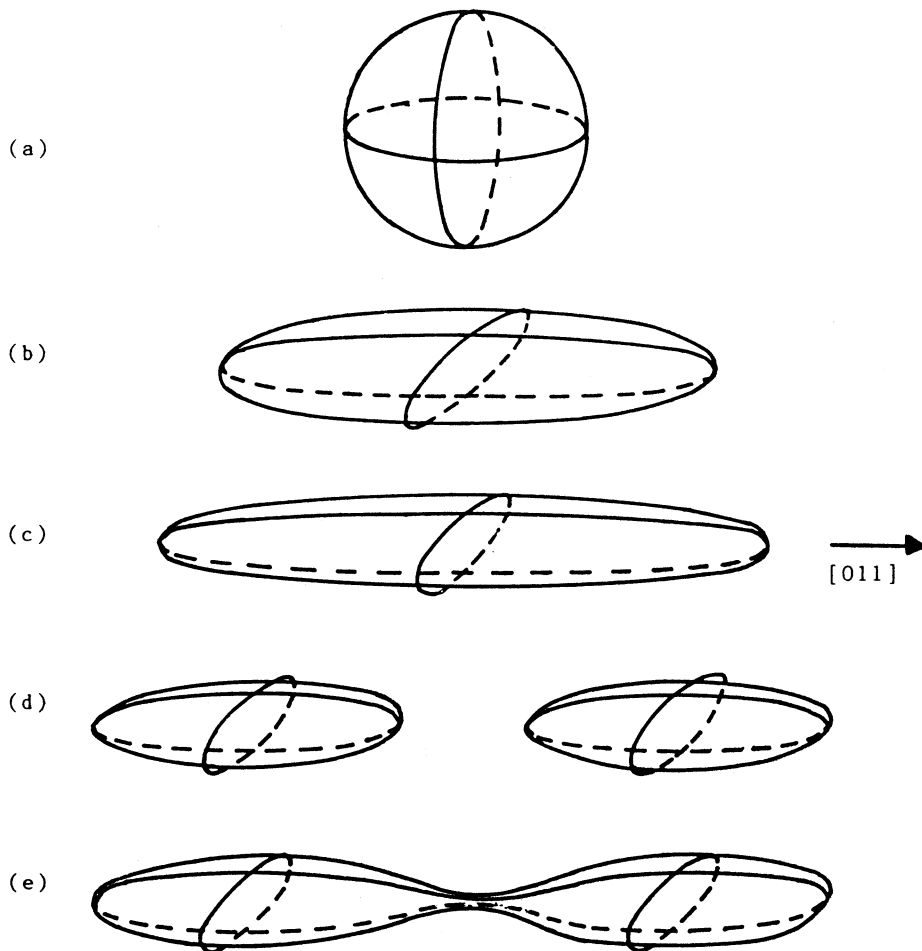


Figure 11. Sketch of the spin-density around the negative vacancy in silicon in increasing degree of detail as deduced from the ENDOR measurements.

net spin on the bc-plane. The resulting distribution of spin density is then as indicated in a sketchy manner in figure 11(e). A theoretical estimate of this exchange-induced polarization phenomenon has produced order-of-magnitude agreement with the experimental observations [13].

REFERENCES

- [1] Watkins G.D., Lattice Defects in Semiconductors 1974 (Inst. Phys. Conf. Ser. 23 1975), p.1.
- [2] Stoneham A.M., Theory of Defects in Solids (Clarendon Press, Oxford, 1975)
- [3] Baraff G.A., Kane E.O. and Schlüter M., Phys.Rev.B21, 5662 (1980)
- [4] Newton J.L., Chatterjee A.P., Harris R.D. and Watkins G.D., Physica 116B, 219 (1983)
- [5] Watkins G.D., J.Phys.Soc.Japan 18, suppl.II. 22 (1963)
- [6] Watkins G.D., Radiation Damage in Semiconductors (Dunod, Paris, 1965), p.97
- [7] Sprenger M., Muller S.H. and Ammerlaan C.A.J., Physica 116B, 224 (1983)
- [8] Watkins G.D., Phys.Rev.B13, 2511 (1976)
- [9] Sprenger M., van Kemp R., Sieverts E.G. and Ammerlaan C.A.J., J.Electron.Mater.14a, 815 (1985)
- [10] Sprenger M., to be published
- [11] Morton J.R. and Preston K.F., J.Magn.Reson.,30, 577 (1978)
- [12] Kane E.O., Phys.Rev.B31, 5199 (1985)
- [13] Lanoo M., Phys.Rev.B28, 2403 (1983).